Chapter 1

Analysis

We analyze ATLAS data to search for events which contain a pair of W bosons with one decaying to $l\nu$ and the other decaying to $q\bar{q}$, and with the pair consistent with having been produced by a new resonance denoted by s (as described in Chapter 2 subsection 2.2). Following the centrally-performed reconstruction of ATLAS proton-proton collision data, we analyze the reconstructed physics objects to search for evidence of new physics in this mono-$s \to WW$ semileptonic channel. This thesis focuses on the design of the most sensitive "merged" signal region of the possible phase space of events, as well as the addition of two control regions to constrain the $t\bar{t}$ background contribution. Other regions used to specify potential signal and the various types of background within the analysis, as well as still further regions used for control and for validation of the analysis, are described in more brief detail in order to provide context to decision-making and a fuller picture of the analysis.

1.1 Cut and Count Analysis

This analysis uses the "cut and count" strategy to search for evidence of the signal model. In order to perform this search, we define a set of selection criteria to slice or "cut" the data according to various event variables, such as the amount of missing transverse momentum. We choose these selection criteria in order to maximize the expected number of signal events, and minimize the expected number of standard model background events in the region, based on the MC simulated data. While designing the selection criteria, real ATLAS data is hidden, or blinded, in order to avoid biasing the selection. The final area of phase space defined by the selection criteria

is known as the "signal region". As the final stage of an analysis, the real ATLAS data can be compared with the simulated MC data, and a statistical conclusion can be reached about the likelihood of the existence of the signal model. The more signal and less background that are present in the signal region, the stronger the statistical evidence for existence of the beyond-SM signal channel will be.

In order to improve the accuracy of the analysis and reduce the uncertainty on the amount of predicted standard model background, a "control region" may also be used. This is a region not overlapping with the signal region which is designed to have similar kinematic properties to signal events, but be more pure in one or more standard model backgrounds and much less rich in actual expected signal events. In this region, we can compare the number of MC simulated background events and ATLAS data events, and any differences provide additional information to correct and constrain the expected number of background events in the signal region.

1.2 Analysis Strategy

In this analysis, there are two analysis channels which are combined statistically during fitting. These channels are distinguished by the reconstruction of the dijet system from the hadronically-decaying W boson, and are named the "merged" channel and the "resolved" channel. In the "merged" channel, we reconstruct the dijet system with a single $R = 1.0$ Track-Assisted-Reclustered (TAR) jet, which generally means that the dijet system is more boosted, with the s decay products closer together. In the less-boosted "resolved" channel we reconstruct the dijet system using a pair of $R = 0.4$ jets. Figure 1.1 provides a visual demonstration of this difference. In each analysis channel there are three analysis regions: the semileptonic signal region, a control region designed to constrain the $t\bar{t}$ background, and a control region designed to constrain the W+jets background. To ensure that "merged" and "resolved" regions do not overlap, an event recycling strategy is employed where only events failing the selection for all "merged" regions are considered for selection in "resolved" regions.

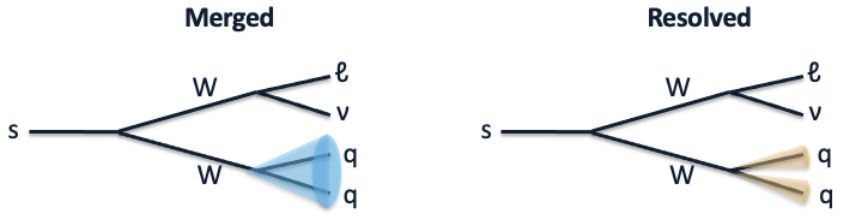

Figure 1.1: Schematic representation of the differing reconstruction technique between merged and resolved regions.

1.3 Merged Signal Region

1.3.1 Signal and Background Characterization

The first step towards defining signal region selection criteria is to characterize signal and background events, while searching for exploitable differences. Event characteristics explored include the relative positions of analysis objects, the transverse momenta and masses of analysis objects, along with various jet substructure variables. Figures **??**, **??**, and **??** in Appendix section **??** show distributions of signal and background events for many of the variables studied at preselection level.

1.3.2 TAR Jet Lepton Disentanglement

Reconstructing the hadronically-decaying W boson as accurately as possible is key in this analysis. As a result, it is given special attention, especially in the more sensitive merged channel. In this channel, the W is reconstructed by a single $R = 1.0$ TAR jet. Due to the boosted nature of the s-decay, however, the leptonically-decaying W often lies in or very near to this jet. As a result, the charged lepton often overlaps the TAR jet, which can lead to difficulty in jet reconstruction.

In order to resolve this difficulty, I made modifications to the TAR jet building process to disentangle overlapping leptons. I identify input tracks and jets that are likely to be attributable to a final state lepton and not the hadronic W decay, and remove them. To achieve this, I remove tracks associated with a baseline electron or muon from the input track collection. I then also remove any anti-k_t $R = 0.2$ jet overlapping with a baseline electron (defined here as having $\Delta R(lep, jet) < 0.2$) prior to reclustering into $R = 1.0$ jets. I do not remove $R = 0.2$ jets overlapping muons,

as muons do not leave large a calorimeter signature and are therefore unlikely to fake hadronic activity. This results in the following updated TAR jet building algorithm, where steps with a (*) are added to disentangle leptons:

- Tracks and calibrated anti-k_t $R = 0.2$ jets are chosen as input to the algorithm.
- Tracks associated with a baseline muon or electron are removed from the input collection (*).
- anti-k_t $R = 0.2$ jets overlapping with a baseline electron ($\Delta R < 0.2$) are removed from the input collection (*).
- The remaining anti-k_t $R = 0.2$ jets are reclustered into $R = 1.0$ jets using the anti-k_t algorithm, and trimmed using the p_T fraction $f_{cut} = 0.05$.
- Input tracks are matched to $R = 0.2$ jets if possible, using ghost association.
- Tracks which remain unassociated are matched to the nearest anti-k_t $R = 0.2$ jet within $\Delta R < 0.3$.
- The p_T of each track is rescaled using the p_T of the jet to which it is matched using the equation:

$$p_T^{\text{track, new}} = p_T^{\text{track, old}} \times \frac{p_T^{\text{subjet } j}}{\sum_{i \in j} p_T^{\text{track } i}}, \tag{1.1}$$

  where j is the $R = 0.2$ subjet that the track being rescaled is matched with, and the index i runs over all tracks matched to that subjet. This rescaling accounts for the momentum of neutral particles (except for neutrinos), which is measured at calorimeter level but is not visible in the tracker.
- Finally, jet substructure variables and m^{TAR} are calculated using the rescaled matched tracks.

In order to study the potential benefit of lepton-disentanglement, I produced near-identical sets of signal MC samples, with one implementing disentanglement and the other not. I then compared the mass of the reconstructed jets in the two samples in a region where a lepton overlaps the $R = 1.0$ TAR Jet ($\Delta R(e, \text{TAR}) < 1$), to determine how well the W boson mass is reconstructed in this case. Figure 1.2 demonstrates the improvement in mass resolution achieved by disentangling leptons from TAR jets. A

clearly enhanced resolution in the TAR jet mass peak around the W mass is visible for the lepton-disentangled jets in the electron channel. This significantly improves sensitivity in the merged signal region by allowing a much tighter selection on the TAR jet mass. Very little changes in the muon channel.

I additionally compared the performance of building the TAR jets from constituent anti-k_t $R = 0.4$ jets, rather than anti-k_t $R = 0.2$ jets. In the electron channel I found that for high s mass, W mass reconstruction performance was similar between the two methods, but for low s mass using anti-k_t $R = 0.4$ jets significantly impairs resolution around the W mass. Again in the muon channel I observed few significant differences. Figure 1.3 shows a comparison of the TAR jet mass distribution built from anti-k_t $R = 0.4$ and anti-k_t $R = 0.2$ jets, for two selected signal points, in a signal-enriched region with 1 electron, $\Delta R(e, \text{TAR}) < 1$, and $m_{\text{T}}(\ell, E_T^{miss}) > 150$ GeV. This clearly demonstrates the improved mass resolution for the signal point at $m_s = 160$ GeV.

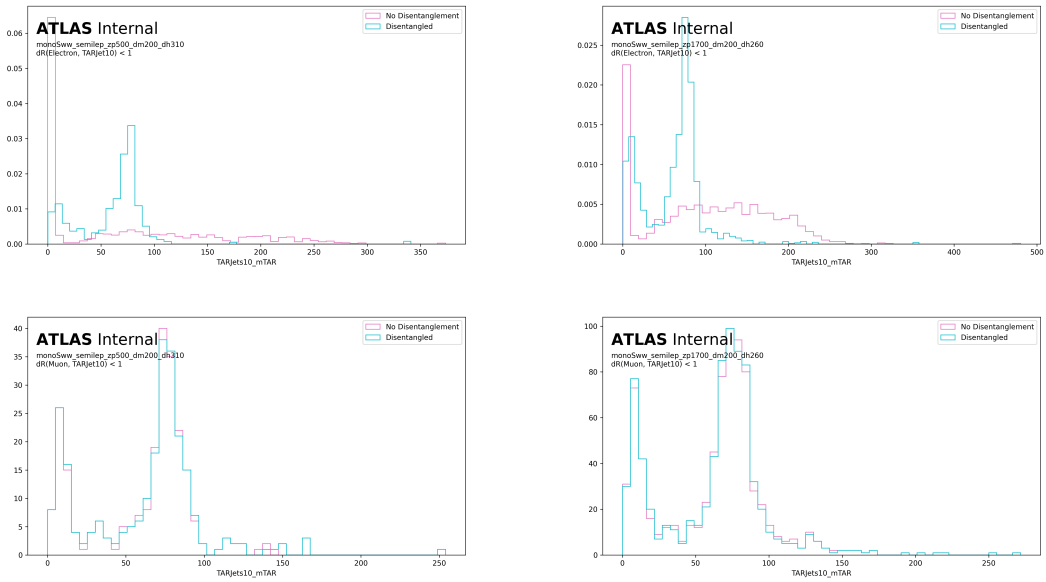

Figure 1.2: Normalized $R = 1.0$ TAR jet mass distributions with and without lepton disentanglement applied for four representative signal points. **Upper row:** electron channel, **lower row:** muon channel.

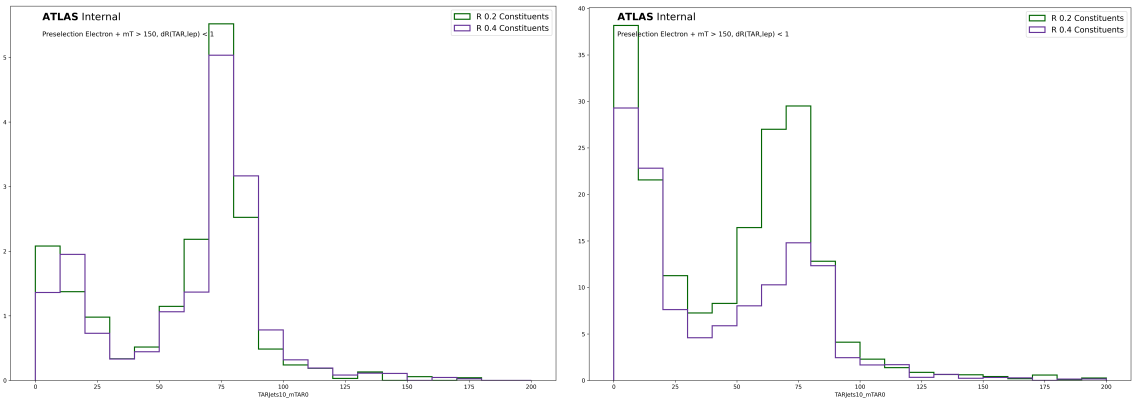

Figure 1.3: TAR jet mass distributions for two representative signal points, compared with constituent anti-k_t $R = 0.4$ vs. anti-k_t $R = 0.2$ jets. Left: sample signal point at $(m_s, m_{Z'}) = (310, 500)$ GeV. Right: sample signal point at $(m_s, m_{Z'}) = (160, 1700)$ GeV.

1.3.3 Merged Signal Region Optimization

Asimov Significance

I optimized the "merged" signal region using the expected Asimov discovery significance Z as the figure of merit [1]. This is given by:

$$Z = \left[2(s+b)\left(\ln\left[\frac{(s+b)(b+\sigma_b^2)}{b^2+(s+b)\sigma_b^2}\right] - \frac{b^2}{\sigma_b^2}\ln\left[1+\frac{\sigma_b^2 s}{b(b+\sigma_b^2)}\right]\right)\right]^{\frac{1}{2}}, \qquad (1.2)$$

where b is the expected total number of background events, s is the expected total number of signal events, and σ_b is the uncertainty on the expected total number of background events. For a given set of selection criteria and signal point, this metric is calculated from the MC simulated data by applying the criteria, counting the number of remaining signal and background events, and computing their uncertainties, then calculating the significance. It provides a metric to assess the expected sensitivity of the signal region to the signal model.

Optimization Approach

In order to optimize the signal region selection, I employed a combination of an iterative visual approach and a computational approach. Visually, I studied the distributions of analysis variables, comparing signal and background distributions, to find areas of good discrimination where a cut placement might improve sensitivity. I

then compiled a list of possible cuts in each of these areas of discrimination to form a basis for the computational optimization. To determine the optimal combination of these possible cuts, I created a script to test all possible combinations while computing the expected Asimov significance of each. When calculating significance during optimization, in addition to statistical uncertainty I applied a flat 20% systematic uncertainty on the number of background events to more realistically reflect the expected total uncertainty. Different signal points in the m_s-$m_{Z'}$ plane have different kinematic properties, and cross-sections and therefore have different optimal selection. As a result, I selected the following four signal points at the edge of the search window for optimization:

- $(m_s, m_{Z'}) = (310 \text{ GeV}, 500 \text{ GeV})$,
- $(m_s, m_{Z'}) = (335 \text{ GeV}, 1000 \text{ GeV})$,
- $(m_s, m_{Z'}) = (285 \text{ GeV}, 1700 \text{ GeV})$,
- and $(m_s, m_{Z'}) = (210 \text{ GeV}, 2100 \text{ GeV})$.

I then considered the cut combination with the highest mean expected Asimov significance over these four points to be optimal. In early iterations of optimization, the number of signal events selected using the optimal selection criteria was undesireably low. As a result, I implemented an additional requirement forcing the chosen criteria to maintain an expected yield of at least 15 signal events in the "merged" signal region.

In order to avoid over-tuning the optimization on single events or statistical fluctuations, I spaced the lattice of possible cuts widely enough to allow several MC events to fall between each placement. Optimizing a selection in this manner also creates a systematic bias toward an under-prediction of background in the signal region, because a low expected background yield is considered desireable. To counter this bias, I used statistically-independent optimization and fitting data sets. I performed all optimization using a set of MC samples produced when using Sherpa 2.2.1 as a training set. A set of samples produced when using Sherpa 2.2.10 then provides a statistically-independent and more statistically rich data set which I used for validation and fit model testing. This means that the MC data used for fit model testing is isolated from the optimization of selection criteria.

Optimization Variables

I examined many analysis variables for potential sensitivity, and selected those having the best discrimination potential to be tested in the final optimization. Presented below is a list of variables tested and their meaning:

- $\boldsymbol{E_T^{miss}}$ and $\mathcal{S}$: Missing transverse momentum; and the significance of its difference from a value of zero.
- $\boldsymbol{p_T(\ell)}$: Transverse momentum of signal lepton.
- $\boldsymbol{m_T(\ell, E_T^{miss})}$: Transverse mass of lepton and E_T^{miss} system, given by

$$m_{\mathrm{T}}(\ell, E_T^{miss}) = \sqrt{2p_{\mathrm{T},\ell}E_T^{miss}\left(1-\cos\left(\phi_\ell - \phi_{E_T^{miss}}\right)\right)} \tag{1.3}$$

- $\boldsymbol{m^{\text{TAR Jet}}}$: Mass of the p_T-leading TAR jet calculated from the rescaled matched tracks.
- $\boldsymbol{p_T^{\text{TAR Jet}}}$: Transverse momentum of the leading TAR jet.
- $\boldsymbol{D_2^{\beta=1}}$**(TAR Jet)**: Energy correlation function of the TAR jet, which helps to identify two-pronged jet substructure [2].
- **TAR Jet** $\boldsymbol{\tau_{42}^{WTA}}$ **and** $\boldsymbol{\tau_{21}^{WTA}}$: "$n$-Subjettiness" ratios of the leading TAR jet, to identify two-pronged substructure [3].

In addition, I considered a two-dimensional cut above or below a line with variable slope and intetcept in the E_T^{miss}-$p_T(\ell)$ plane during optimization.

Optimized Selection

I found the maximum mean expected significance across the four selected signal points to be achieved using the selection shown in Table 1.1.

In order to validate this choice of selection criteria, I produced "$N-1$" plots which show the distribution of a variable with all but the cut on that variable applied. I also calculated the expected Asimov significance of placing a cut at each bin edge in the "$N-1$" histogram. I then compared the optimized cut placement with the cut placement showing maximal expected significance in the plot. These plots were produced using the testing and validation data (W+jets and Z+jets samples produced

variable	**requirement**	**reason**
N(TAR Jets)	> 0	W_{Cand} reconstruction
$m_{\text{T}}(\ell, E_T^{miss})$	$> 220\,GeV$	W+jets background reduction
$m^{\text{TAR Jet}}$	$[68, 89]\,GeV$	W_{Cand} reconstruction
$\mathcal{S}$	> 16	Select for high E_T^{miss}
ΔR(TAR Jet, ℓ)	< 1.2	Select for boosted W_{Cand} $+\ell\nu$ system
$D_2^{\beta=1}$(TAR Jet)	< 1.1	2-pronged $W \to qq$ reconstruction

Table 1.1: Optimized selection criteria for the "merged" category signal region.

in Sherpa 2.2.10), and are shown in Figure 1.4. They show that the cuts optimized using Sherpa 2.2.1 samples are still placed at optimal or near-optimal locations using the final samples, and therefore validate the choice of selection criteria.

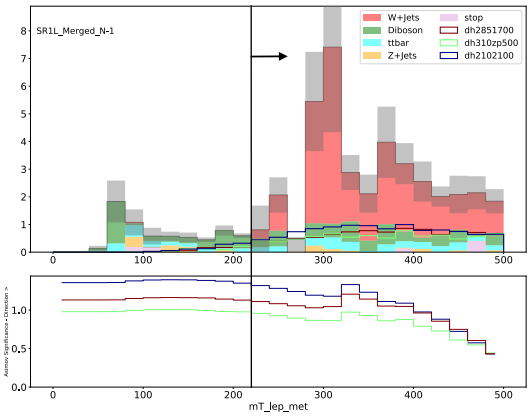

(a) $m_{\mathrm{T}}(\ell, E_T^{miss})$

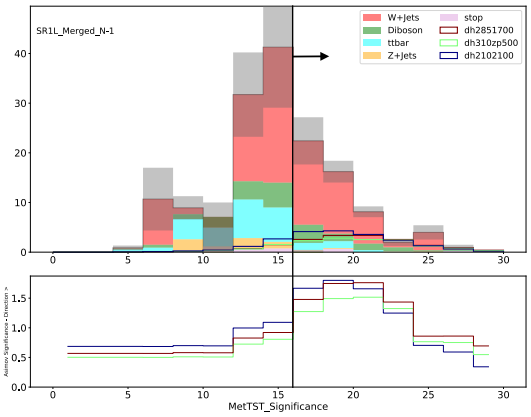

(b) $\mathcal{S}$

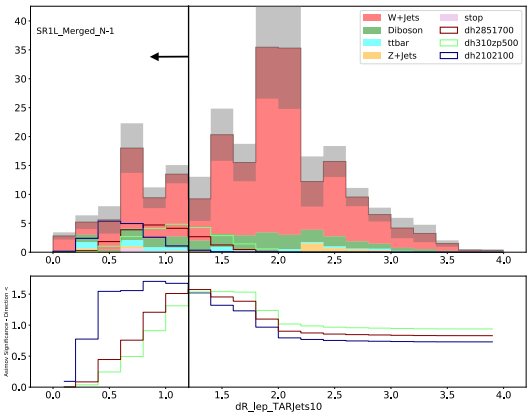

(c) $\Delta R(\text{TAR Jet}, \ell)$

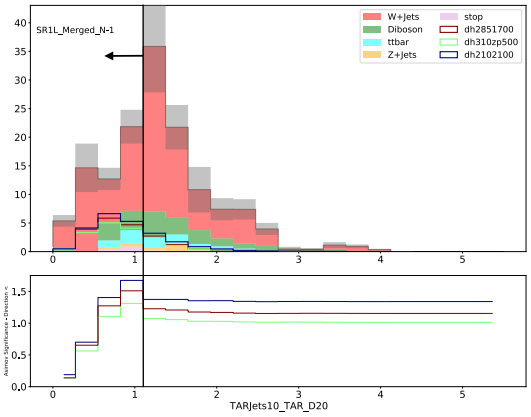

(d) $D_2^{\beta=1}(\text{TAR Jet})$

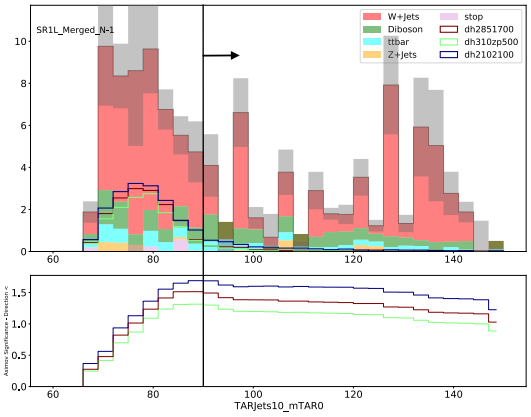

(e) $m^{\text{TAR Jet}}$

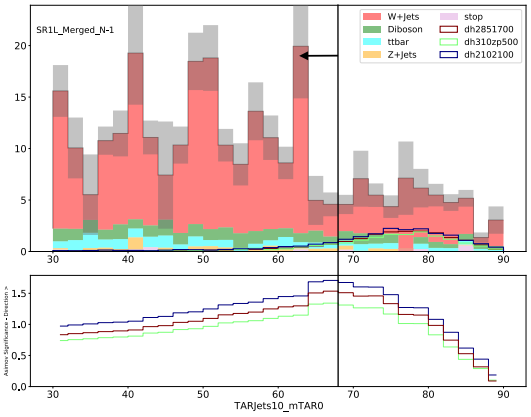

(f) $m^{\text{TAR Jet}}$

Figure 1.4: $N-1$ plots in the "merged" signal region.

1.4 Resolved Signal Region

Due to the highly boosted nature of most signal events, the hadronic W decay products are often best resconstructed as an $R = 1.0$ TAR jet. To capture events for which this is not the best reconstruction we define our "resolved" signal region. Being a secondary region, the "resolved" signal region is considerably less sensitive to the signal model than the "merged" signal region, but does provide some enhancement especially at low s mass where the least boost is experienced. The "resolved" signal region selection criteria are listed in Table 1.2.

Table 1.2: Overview of "resolved" SR cuts.

cut	**reason**
Fails "merged" analysis region selections	Recycling strategy
$N(\text{Jets}) \geq 2$	W_{Cand} reconstruction
$m(W_{\text{Cand}}) \in [60, 100]\ GeV$	W_{Cand} reconstruction
$p_T(W_{\text{Cand}}) > 100\ GeV$	W+jets Background Reduction
$m_{\text{T}}(\ell, E_T^{miss}) > 200\ GeV$	W+jets Background Reduction
$\mathcal{S} > 14$	Select for high E_T^{miss}
$\Delta R(W_{\text{Cand}}, \ell) < 1.75$	Select for boosted W_{Cand} $+\ell\nu$ system

1.5 $t\bar{t}$ Control Regions

A control region is used to help constrain one or more sources of background in an analysis. It is designed as a region that covers a similar but non-overlapping area of phase space to the signal region, and is expected to contain many fewer signal events. As a result, the number of observed ATLAS data and MC-predicted SM events should match very closely. Any difference provides information about how MC predictions differ from data observations and is used derive a normalization factor to constrain the SM background predictions of MC in the signal region, and provide a more accurate projection.

To design an effective control region, I attempted to satisfy four important criteria:

- **Non-overlap with the signal region:** This ensures that the sample used to constrain the signal region background is statistically-independent from the signal region.

- **High $t\bar{t}$ purity:** This selects for the background of interest in the control region to better individually constrain that background.
- **Low signal contamination:** This ensures that the comparison of ATLAS data and MC in this region is not affected by the signal model and effectively constrains only the SM background.
- **Similar kinematics to SR:** This ensures that a similar region of phase space is being studied in the control and signal regions, so that the normalization factors derived apply well to both regions.

The fact that $t\bar{t}$ is one of the sub-dominant backgrounds in both signal regions motivated me to create one such control region for each signal region. As a consequence of top quarks decaying primarily to a W boson and b-quark, the principal cut excluding $t\bar{t}$ events from the signal regions is the veto of any events containing a b-tagged anti-k_t $R = 0.4$ jet. I therefore chose to try defining a similar but non-overlapping region rich in $t\bar{t}$ events by simply reversing this cut and also requiring at least 1 b-tagged jet. I found this proposed region to be too rich in expected signal events, however, with signal yields as high as 10% of background yields in the "merged" region.

To improve this, I further extended the b-jet cut to require 2 or more b-jets in the control region. This change sufficiently reduced signal contamination, but in the "merged" control region it had the additional consequence of substantially reducing the number of events in the region, thereby reducing its statistical power. In response I also loosened the $\mathcal{S}$ cut in the "merged" $t\bar{t}$ control region to $\mathcal{S} > 12$, considerably improving the $t\bar{t}$ yield. To inform this choice, I used figure 1.5, which shows the number of weighted $t\bar{t}$ events expected within the "merged" control region for a given $\mathcal{S}$ cut.

Table 1.3 summarizes the differences in selection criteria between the "merged" and "resolved" signal and $t\bar{t}$ control regions. Figures **??** and **??** in Appendix section **??** show comparisons of the distributions of MC and ATLAS data in the $t\bar{t}$ control regions. These demonstrate a slight over-prediction of background from MC in the "merged" region, which is used during fitting to constrain the $t\bar{t}$ background in the signal region. The difference between data and MC distributions does not show a strong correlation with any of the analysis variables. To ensure that the kinematic qualities of the signal and control regions are sufficiently similar to provide a good

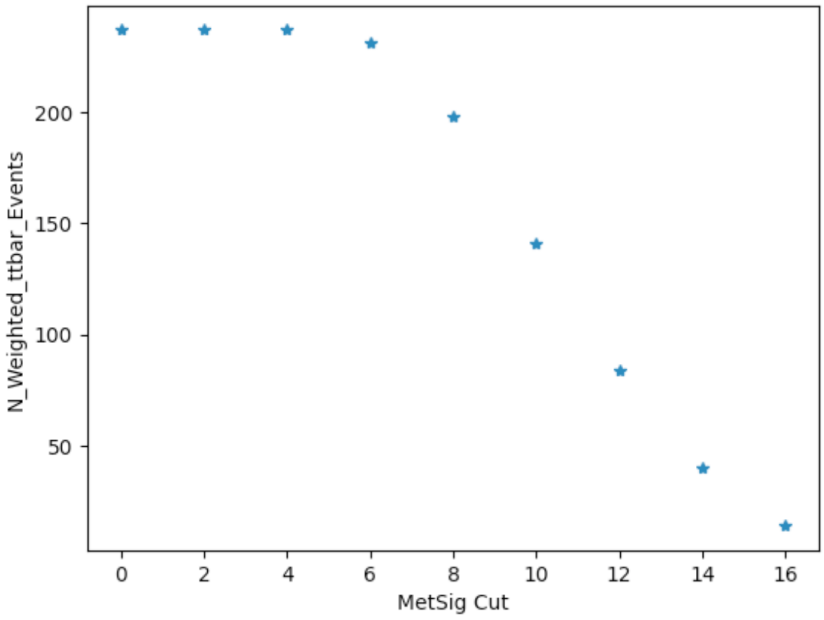

Figure 1.5: $t\bar{t}$ yield in the "merged" $t\bar{t}$ control region for various E_T^{miss} significance cut placements.

Region	$N(b\text{-jets})$ Cut	$\mathcal{S}$ Cut
Merged SR	$N(b\text{-jets}) = 0$	$\mathcal{S} > 16$
Resolved SR	$N(b\text{-jets}) = 0$	$\mathcal{S} > 14$
Merged CRtt	$N(b\text{-jets}) > 1$	$\mathcal{S} > 12$
Resolved CRtt	$N(b\text{-jets}) > 1$	$\mathcal{S} > 14$

Table 1.3: Summary of differences in selections on $N(b\text{-jets})$ and $\mathcal{S}$ between signal regions and $t\bar{t}$ control regions.

constraint, Figures **??** and **??** in Appendix section **??** show comparisons of distributions of key kinematic variables between the "merged" and "resolved" control and signal regions.

1.6 W+jets Control Region

This analysis employs an additional pair of control regions in order to constrain the dominant W+jets background in the signal regions. The signal regions occupy a realm of phase space very high in $m_{\mathrm{T}}(\ell, E_T^{miss})$, and we sought to better constrain the background prediction in the tail of this distribution. To achieve this we defined control regions by reversing the $\Delta R(\text{TAR Jet}, \ell)$ and $\Delta R(W_{\text{Cand}}, \ell)$ cuts in the "merged" and "resolved" signal regions. This reverses the direction of the neutrino and charged lepton in the leptonic W decay without substantially altering the remaining kinematics of the event, keeping the region high in $m_{\mathrm{T}}(\ell, E_T^{miss})$. In the "merged" W+jets control region we again reduced the $\mathcal{S}$ cut to $\mathcal{S} > 12$ in order to improve statistical power. Table 1.4 summarizes the differences in selection criteria between the "merged" and "resolved" signal and W+jets control regions.

Region	ΔR Cut	$\mathcal{S}$ Cut
Merged SR	$\Delta R(\text{TAR Jet}, \ell) < 1.2$	$\mathcal{S} > 16$
Resolved SR	$\Delta R(W_{\text{Cand}}, \ell) < 1.75$	$\mathcal{S} > 14$
Merged CRW	$\Delta R(\text{TAR Jet}, \ell) > 1.2$	$\mathcal{S} > 12$
Resolved CRW	$\Delta R(W_{\text{Cand}}, \ell) > 1.75$	$\mathcal{S} > 14$

Table 1.4: Summary of differences in selections on $\Delta R(W_{\text{Cand}}, \ell)$ and $\mathcal{S}$ between signal regions and W+jets control regions.

Figures **??** and **??** in Appendix section **??** show checks of the distributions of MC and ATLAS data in the $W+$jets control regions. As in the $t\bar{t}$ control regions, no strong correlation is observed with any particular variable.

1.7 Trigger Strategy

The ATLAS High Level Triggers (HLT) each represent a set of criteria used by the L2 trigger and event filter to select which events passing the L1 trigger are potentially interesting and should be further analyzed. Throughout the process of optimization and signal and control region definition, we used the unprescaled E_T^{miss} triggers listed in Table 1.5, which select events with high E_T^{miss}. Upon closer examination, however, we found that these triggers were unexpectedly inefficient even in our analysis regions with $E_T^{miss} > 200$ GeV. Figures 1.6 and 1.7 show the E_T^{miss} trigger efficiency in the $t\bar{t}$ control regions in the electron and muon decay channels. In the electron channel we observe full efficiency, but not in the muon channel.

We hypothesized that the inefficiency was caused by high-p_T muons, which are not seen by the trigger-level E_T^{miss} calculation. As a result, if a muon travels in the opposite direction to the true E_T^{miss}, the trigger-level E_T^{miss} will be reduced and the trigger criteria may be failed. To confirm this, Figure 1.8 shows the E_T^{miss} trigger efficiency plotted against E_T^{miss} with signal muons treated as invisible (i.e. having their p_T subtracted from the E_T^{miss}). In this case full or near-full trigger efficiency for $E_T^{miss} > 200$ GeV is recovered. We find it desireable to obtain full trigger efficiency in order to avoid the uncertainty associated with calculating trigger scale factors to match the trigger behaviour of data and MC events. Therefore, to counter the trigger inefficiency we moved to a logical OR between the unprescaled E_T^{miss} triggers and the single muon triggers in Table 1.6. This is designed to ensure that the events with a high-p_T muon that fail the E_T^{miss} trigger will pass the single muon trigger and be considered. Figure 1.9 shows that this recovers full trigger efficiency.

Period	MET Trigger
2015	HLT_xe70_mht
2016 (A-D3)	HLT_xe90_mht_L1XE50
2016 (D4-F1)	HLT_xe100_mht_L1XE50
2016 (F2-)	HLT_xe110_mht_L1XE50
2017 (B-D5)	HLT_xe110_pufit_L1XE55
2017 (D6-K)	HLT_xe110_pufit_L1XE50
2018 (B-C5)	HLT_xe110_pufit_xe70_L1XE50
2018 (C5-)	HLT_xe110_pufit_xe65_L1XE50

Table 1.5: ATLAS unprescaled E_T^{miss} triggers used in Run-2 data-taking.

Periods	Single Muon Trigger
2015	HLT_mu20_iloose_L1MU15
2016 (A, B-D3, D4-E, F-G2, G3-I3, I4-), 2017 (B-), 2018	HLT_mu50
2016	HLT_mu24_iloose
2015, 2016 (A)	HLT_mu40
2016 (B-D3, D4-E)	HLT_mu24_ivarmedium
2016 (D4-E, F-G2, G3-I3, I4-), 2017 (B-), 2018	HLT_mu26_ivarmedium

Table 1.6: ATLAS single muon triggers used in Run-2 data taking.

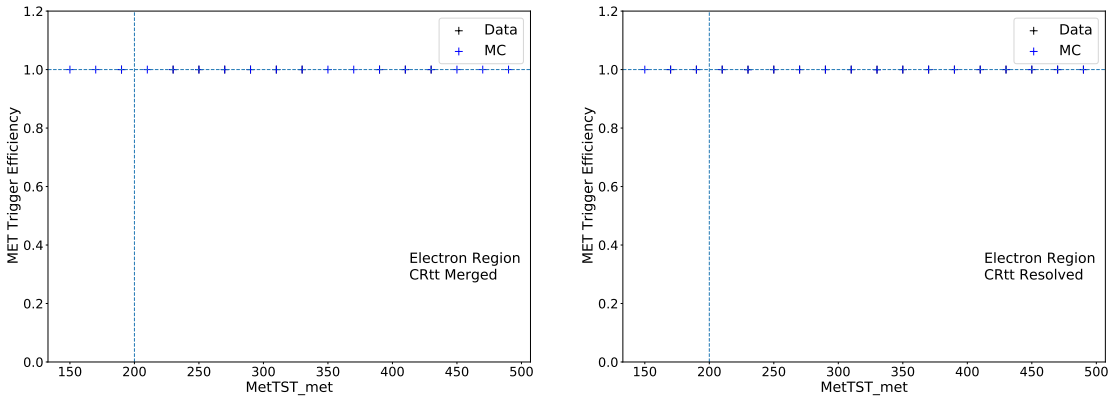

(a) $t\bar{t}$ CR Merged (b) $t\bar{t}$ CR Resolved

Figure 1.6: E_T^{miss} trigger efficiency in the electron channel.

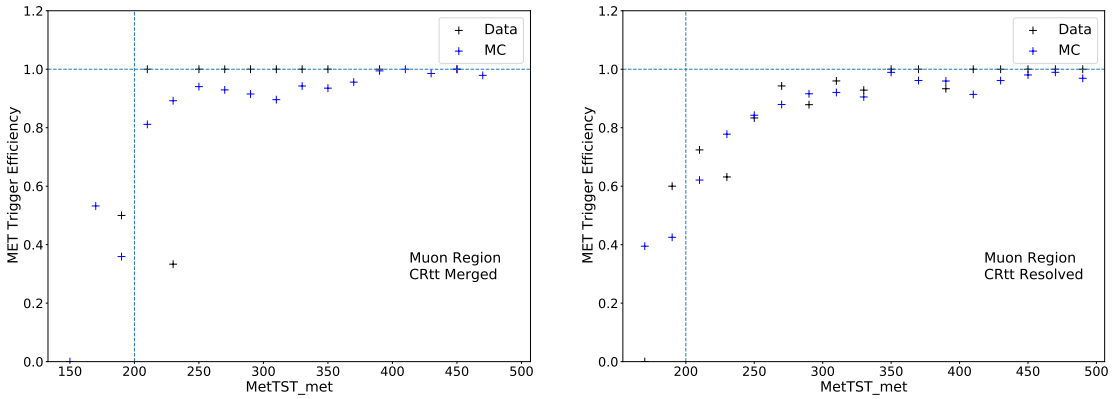

(a) $t\bar{t}$ CR Merged (b) $t\bar{t}$ CR Resolved

Figure 1.7: E_T^{miss} trigger efficiency in the muon channel.

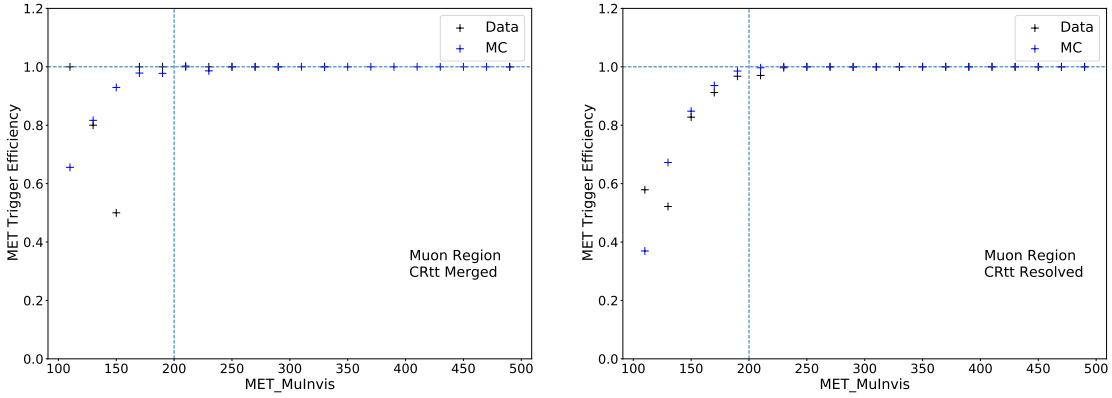

(a) $t\bar{t}$ CR Merged (b) $t\bar{t}$ CR Resolved

Figure 1.8: E_T^{miss} trigger efficiency plotted against E_T^{miss} with muons invisible.

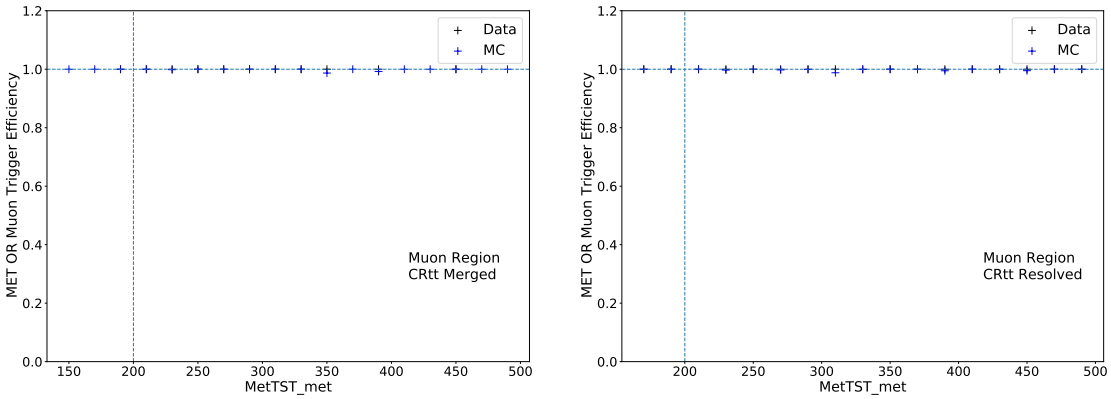

(a) $t\bar{t}$ CR Merged (b) $t\bar{t}$ CR Resolved

Figure 1.9: Efficiency of the logical OR of E_T^{miss} and signle muon triggers.

Bibliography

1. Cowan, G., Cranmer, K., Gross, E. & Vitells, O. Asymptotic formulae for likelihood-based tests of new physics. *Eur. Phys. J. C* **71.** [Erratum: Eur.Phys.J.C 73, 2501 (2013)], 1554. arXiv: `1007.1727 [physics.data-an]` (2011).
2. Larkoski, A. J., Salam, G. P. & Thaler, J. Energy Correlation Functions for Jet Substructure. *JHEP* **06,** 108. arXiv: `1305.0007 [hep-ph]` (2013).
3. Aaboud, M. *et al.* Measurement of jet-substructure observables in top quark, W boson and light jet production in proton-proton collisions at $\sqrt{s} = 13$ TeV with the ATLAS detector. *JHEP* **08,** 033. arXiv: `1903.02942 [hep-ex]` (2019).